Astron. Astrophys. 325, 341–351 (1997)

ASTRONOMY
AND
ASTROPHYSICS

# Convection driven heating of the solar middle chromosphere by resistive dissipation of large scale electric currents. II

**Michael L. Goodman**

Computer Sciences Corporation, Code 695, NASA Goddard Space Flight Center, Greenbelt, Maryland 20771, USA
(goodman@spof02.gsfc.nasa.gov)

Received 5 February 1997 / Accepted 20 March 1997

**Abstract.** A generalization of a recently developed MHD model of a proposed heating mechanism for the middle chromosphere is presented. The generalization consists of including the ideal gas equation of state, allowing the temperature to vary with position, and allowing the hydrogen flow velocity to vary with height in a specified manner. These generalizations allow for a self consistent calculation of a temperature profile. The variation of the flow velocity with height generates a component of the inertial force which adds to the vertical gradient of the thermal pressure in supporting the plasma against gravity. This allows for a lower temperature for a given number density. The solutions presented suggest that resistively heated magnetic loops embedded in a much stronger, larger scale potential field, and having horizontal spatial scales of several thousand kilometers provide the thermal energy necessary to heat the middle chromosphere on these spatial scales. For these solutions the temperature is in the range of 6000 - 8700 K, consistent with the temperature range in the middle chromosphere. The magnetic loops have one footpoint region where the field is strongest and directed mainly upward, and where the heating rates per unit mass and volume are small. The field lines extend upward from this region at the base of the middle chromosphere, diverge horizontally, and return to a footpoint region at the base of the middle chromosphere as a weaker, more diffuse, mainly downward directed field. In this footpoint region the heating rates are also small. The heating rates are largest in the middle of the loops. For the magnetic loops considered, the temperature shows little horizontal variation between the footpoint region where the field is strongest and the heating rates are small, and the region where the heating rates are largest. This suggests that large horizontal variations in the net radiative loss from heated magnetic loops may not always be associated with large horizontal variations in temperature.

**Key words:** Sun: chromosphere – Sun: magnetic fields – Sun: atmosphere – magnetic fields: plasmas

*Send offprint requests to*: Michael L. Goodman

## 1. Introduction

Goodman (1997) presents a two dimensional, steady state, resistive MHD model with flow to support the proposition that a major source of heating for the middle chromosphere is resistive dissipation of large scale electric currents driven by a convection electric field. The currents are large scale in that their scale heights range from hundreds of kilometers in the network to thousands of kilometers in the internetwork. The current is carried by protons, and flows orthogonal to the magnetic field in a weakly ionized, strongly magnetized hydrogen plasma. The flow velocity is mainly parallel to the magnetic field. The relatively small component of flow velocity orthogonal to the magnetic field generates a convection electric field which drives the current. The magnetic field is the sum of a loop shaped field, called a magnetic element, and a stronger, larger scale potential field. All of the heating takes place in the magnetic element. Solutions to the model indicate that magnetic elements with horizontal spatial extents of $\sim 1 - 5 \times 10^3$ km may be confined to, and heat, the middle chromospheric network. Other solutions to the model indicate that magnetic elements with horizontal spatial extents of $\sim 1 - 3 \times 10^4$ km may span and heat the middle chromospheric internetwork over the interior of supergranules, and may be the building blocks of the chromospheric magnetic canopy.

The model in Goodman (1997) does not include an equation of state, assumes that the temperature is constant, and assumes that the hydrogen flow velocity does not vary with height. The model presented here generalizes that model by including the ideal gas equation of state, allowing the temperature to vary with position, and allowing the hydrogen flow velocity to vary with height in a specified manner. The temperature range of the model solutions discussed in Sect. 5 is 6000 - 8700 K which is essentially the temperature range that identifies the middle chromosphere. These solutions describe the properties of resistively heated magnetic loops with horizontal spatial extents of $\sim 1900 - 2600$ km.

The model is restricted to the middle chromosphere, which in the internetwork is believed to be co - spatial with the magnetic canopy (Solanki et al. 1994), and which in the network

is known to be co - spatial with magnetic fields rooted in kilogauss strength flux tubes in the underlying photosphere. Numerous observations suggest a strong positive correlation between magnetic field strength and heating rate throughout the middle chromosphere (as well as in the upper chromosphere, transition region and corona). It is virtually certain that the magnetic field plays a major role in the mechanism(s) that heat the entire middle chromosphere. While the model proposes a resistive heating mechanism for the middle chromosphere in the network and internetwork, the mechanisms responsible for heating the lower chromosphere may be of a different nature. Acoustic wave dissipation is a possible mechanism for heating the lower chromosphere in regions where the magnetic field is weak, defined by the condition that $\beta \gg 1$ where $\beta$ is the ratio of the plasma pressure to the magnetic pressure (Rammacher & Ulmschneider 1992; Ulmschneider, Priest & Rosner 1991; Carlsson & Stein 1995, 1994, 1992). In particular, Carlsson & Stein propose that the regions of the lower internetwork chromosphere where the magnetic field is weak are heated by the hydrodynamic mechanism of the viscous dissipation of, and the compression due to, acoustic shock waves. Observations by Lin (1995) indicate the presence of magnetic flux tubes in the photospheric internetwork with an average field strength of 500 G. The field of some of these flux tubes may extend into the lower chromosphere, and play a role in its heating. A causal connection between regions of relatively strong magnetic field and heating in the lower internetwork chromosphere is suggested by Sivaraman & Livingston (1982) and Kalkofen (1996). Although most of the lower chromospheric internetwork may be practically field free and heated by a purely hydrodynamic mechanism, it is likely that the relatively small area occupied by strong flux tubes, such as those detected by Lin (1995), is heated by a magnetic field related mechanism. This follows by analogy with the chromospheric network where there is a strong positive correlation between heating and the magnetic field strength of the underlying photospheric flux tubes, which is $\sim 1000 - 1500$ G, only 2 - 3 times larger than the average field strength of the strong photospheric flux tubes observed by Lin (1995) in the internetwork.

The model is steady state, and so cannot model chromospheric intensity oscillations. Observed oscillations have periods ranging from $\sim 3$ minutes in the internetwork to $\sim 5 - 20$ minutes in the network, and correspond to velocity fluctuations up to $\sim 2$ km-sec$^{-1}$ (von Uexküll & Kneer 1995; Bocchialini et al. 1994; Lites 1994; Lites et al. 1993; Kneer & von Uexküll 1993; Kulaczewski 1992; Deubner & Fleck 1990). Although the real chromosphere is dynamic, steady state models provide a tractable way of studying many of its important properties. In particular, the model presented here provides a relatively simple way of studying many of the main features of the proposed heating mechanism. This mechanism certainly operates throughout the entire chromosphere since any process, such as wave motion, return flow from spicules, downflows resulting from radiative condensation in the upper atmosphere, or magnetic loops rising through the chromosphere, which can drive flow across the magnetic field generates a convection electric field which drives current that is resistively dissipated. The contribution of this mechanism to chromospheric heating remains to be determined. The model presented here is the latest of a series of increasingly realistic models designed to determine this contribution as accurately as is practically possible from the standpoint of MHD modeling.

## 2. Basic equations

Cylindrical coordinates $(R, \theta, Z)$ are used where $R$ measures horizontal distance parallel to the photosphere and $Z$ measures distance from the center of the Sun along a radial line. All quantities are assumed to be independent of $\theta$ and time. Let $\boldsymbol{B}$ and $\boldsymbol{V}$ be the magnetic field and hydrogen flow velocity. It is assumed that $B_\theta = V_\theta = 0$. For the solutions discussed in Sect. 5 the protons are magnetized, defined by the condition that $(\omega_{\rm p}\tau_{\rm pH})^2 \gg 1$ where $\omega_{\rm p}$ and $\tau_{\rm pH}$ are the proton cyclotron frequency and the proton - hydrogen collision time. When the protons are magnetized they carry most of the current orthogonal to the magnetic field in the weakly ionized middle chromospheric hydrogen gas (Chapman & Cowling 1970). The basic equations are as follows.

The mass conservation equation is

$$\frac{1}{R}\frac{\partial(R\rho V_R)}{\partial R} + \frac{\partial(\rho V_Z)}{\partial Z} = 0 \tag{1}$$

where $\rho$ is the hydrogen mass density.

The momentum conservation equation is

$$\rho\left(V_R\frac{\partial V_R}{\partial R} + V_Z\frac{\partial V_R}{\partial Z}\right) + \frac{\partial p}{\partial R} = \frac{J_\theta B_Z}{c} \tag{2}$$

$$\rho\left(V_R\frac{\partial V_Z}{\partial R} + V_Z\frac{\partial V_Z}{\partial Z}\right) + \frac{\partial p}{\partial Z} = -\frac{J_\theta B_R}{c} - \rho g \tag{3}$$

where $p$, $\boldsymbol{J}$, and $c$ are the hydrogen pressure, current density, and speed of light, and $g = 2.74 \times 10^4$ cm-sec$^{-2}$ is the gravitational acceleration which does not vary significantly over the height ranges considered.

Ampere's law is

$$\frac{\partial B_R}{\partial Z} - \frac{\partial B_Z}{\partial R} = \frac{4\pi J_\theta}{c} \tag{4}$$

$$J_R = J_Z = 0. \tag{5}$$

The divergence free condition on $\boldsymbol{B}$ is

$$\frac{1}{R}\frac{\partial(RB_R)}{\partial R} + \frac{\partial B_Z}{\partial Z} = 0. \tag{6}$$

Ohm's law is

$$\boldsymbol{E} + \frac{\boldsymbol{V}\times\boldsymbol{B}}{c} = \eta J_\theta \hat{\theta} \tag{7}$$

where $\boldsymbol{E}$ is the electric field and $\eta$ is the Pedersen resistivity for protons, defined as the inverse of the Pedersen conductivity derived by Chapman & Cowling (1970), and given by

$$\eta = \frac{1}{n_{\rm p} n_{\rm H} e^2 \sigma}\left(\frac{m_{\rm p}^3}{k_{\rm B}T}\right)^{1/2}\left((n_{\rm H}\sigma)^2\frac{k_{\rm B}T}{m_{\rm p}} + \left(\frac{eB}{m_{\rm p}c}\right)^2\right). \tag{8}$$

Here $n_{\rm p}$, $n_{\rm H}$, $e$, $\sigma_{\rm pH}$, $m_{\rm p}$, $k_{\rm B}$, and $T$ are the proton and hydrogen number densities, proton charge, proton - hydrogen scattering cross section, proton mass, Boltzmann's constant, and temperature. $\sigma_{\rm pH}$ is fixed at the value $5 \times 10^{-15}$ cm$^2$ (Book 1994). Equation (8) is valid for all values of $B$. $\eta$ is assumed to be constant, as is the proton density which is an input to the model. The value of $\eta$ for a given solution is determined by the inputs to the model, discussed in Sect. 5.

Ohm's law (7) may be written as

$$E_\theta + \frac{(V_Z B_R - V_R B_Z)}{c} = \eta J_\theta \quad (9)$$

$$E_R = E_Z = 0. \quad (10)$$

Since $\nabla \times \boldsymbol{E} = 0$, and since $E_\theta$ must be finite at $R = 0$, it follows that $E_\theta = 0$. Hence the total electric field is zero, and the current is completely driven by the convection electric field $E_{c\theta} \equiv (V_Z B_R - V_R B_Z)/c$.

The equation of state is

$$p = \frac{\rho k_{\rm B} T(R)}{m_{\rm p}}. \quad (11)$$

The temperature is assumed to be independent of height, consistent with the slow variation of temperature with height in the middle chromosphere predicted by standard semi - empirical, one - dimensional, hydrostatic models of the chromosphere (Anderson & Athay 1989a; Avrett 1984; Vernazza et al. 1981).

The assumed energy equation states that the rate of resistive dissipation is equal to a function $F(R)$ assumed to describe the distribution of the net radiative loss over the magnetic structures being modeled. The energy equation is

$$F(R) = \int_{Z_0}^{\infty} \eta {J_\theta}^2 \, dZ \quad (12)$$

where $Z_0$ is the height of the base of the middle chromosphere, currently thought to be $\sim$ 1000 km. The spatial average of $F$ over the area of the base of the magnetic element is an input to the model. As demonstrated by Goodman (1997) thermal conduction is not an important mechanism for cooling or heating the middle chromosphere because it is too cool. At middle chromospheric temperatures an unphysically large temperature gradient of at least $10^7$ K-km$^{-1}$ is necessary to drive a thermal energy flux comparable to the middle chromospheric net radiative loss of $\sim 10^7$ ergs-cm$^{-2}$-sec$^{-1}$.

## 3. Assumed form of solution

### *3.1. Height dependence*

The general forms of the density, pressure, magnetic field, and velocity are assumed to be given by

$$\rho(R, Z) = \rho_0(R) {\rm e}^{-(Z-Z_0)/L} \quad (13)$$

$$p(R, Z) = p_0(R) {\rm e}^{-(Z-Z_0)/L} \quad (14)$$

$$B_R(R, Z) = b_R(R) {\rm e}^{-(Z-Z_0)/2L} \quad (15)$$

$$B_Z(R, Z) = b_Z(R) {\rm e}^{-(Z-Z_0)/2L} \quad (16)$$

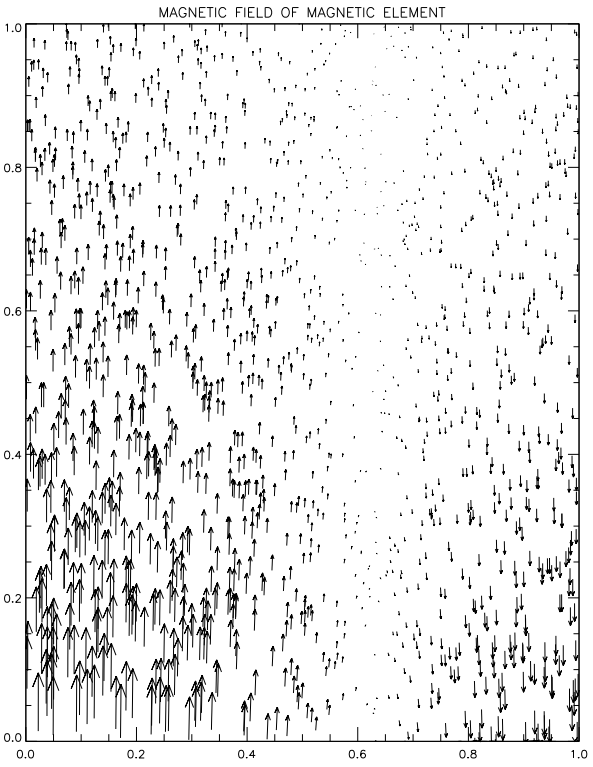


**Fig. 1.** Magnetic field vectors of the magnetic element of solution b. The horizontal axis measures normalized distance $R/2651$ km parallel to the photosphere from the center of the element at $R = 0$. The vertical axis measures normalized height $(Z - Z_0)/3600$ km above the base of the middle chromosphere. The length of the vectors is proportional to the field strength. The magnetic field of solution a has the same basic geometry.

$$V_R(R, Z) = v_R(R) {\rm e}^{-(Z-Z_0)/2L_{\rm V}} \quad (17)$$

$$V_Z(R, Z) = v_Z(R) {\rm e}^{-(Z-Z_0)/2L_{\rm V}} \quad (18)$$

where the scale heights $L$ and $L_{\rm V}$ are assumed constant, and are inputs to the model. It is assumed that $L_{\rm V} \gg L$ so the variation of the inertial force with height is determined mainly by the variation of density with height. The assumed form of the height variation of the velocity is viewed as a first step towards determining the role of a height dependent velocity in the proposed heating mechanism. By assumption $L_{\rm V} > 0$ so the flow speed decreases with increasing height in the middle chromosphere. No solutions are found for $L_{\rm V} < 0$. For the solutions discussed in Sect. 5 it is assumed that $L_{\rm V} = 8L$ so the flow velocity is almost constant over several pressure scale heights.

The assumed form for $\boldsymbol{V}$ given by Eqs. (17) and (18) is substituted into the basic equations, and all differentiations with respect to $Z$ are performed. Then, using the assumption that $L_{\rm V} \gg L$, the exponential factor describing the dependence of $\boldsymbol{V}$ on $Z$ is dropped. All that remains of the height dependence of $\boldsymbol{V}$ in the final equations to be solved are terms involving factors of $1/L_{\rm V}$.

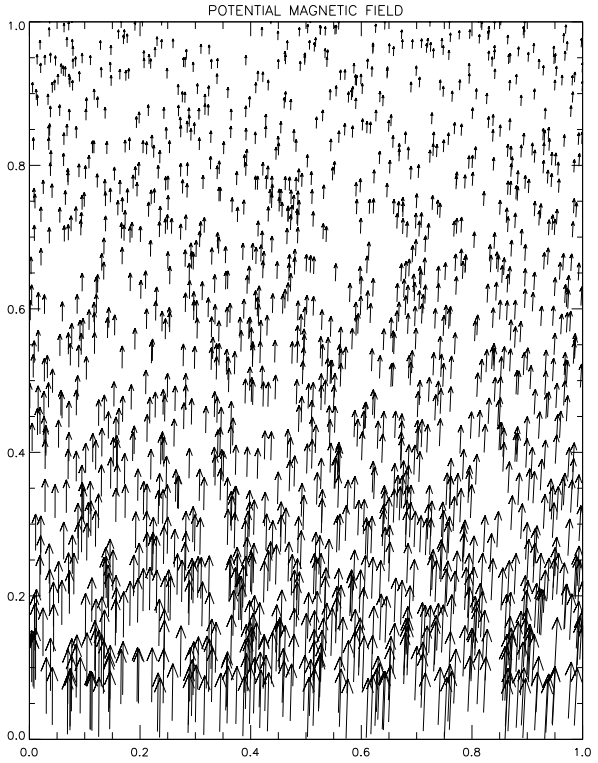


**Fig. 2.** Magnetic field vectors of the potential magnetic field of solution b. The axis definitions and normalizations are the same as for Fig. 1. The potential magnetic field of solution a has the same basic geometry.

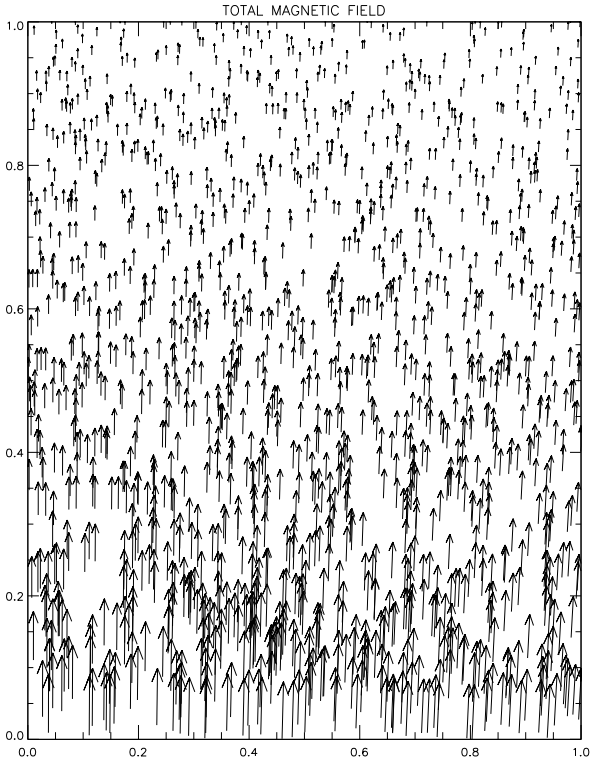


**Fig. 3.** Magnetic field vectors of the total magnetic field of solution b. The axis definitions and normalizations are the same as for Fig. 1. The total magnetic field of solution a has the same basic geometry.

### *3.2. Magnetic field*

The magnetic field geometry is specified as the sum of a loop shaped structure, called a magnetic element, and a potential magnetic field. Let $b_R = b_{1R} + b_{2R}$, and $b_Z = b_{1Z} + b_{2Z}$ in Eqs. (15) and (16), where the subscripts 1 and 2 refer to the loop magnetic field and the potential magnetic field.

The equations for the $R$ and $Z$ components of the magnetic field of the magnetic element, and its associated current density, are obtained from Eqs. (21) - (23) in Goodman (1996). Setting $t = Z - Z_0 = 0$ in these equations gives

$$b_{1R} = \frac{B_1 R_\mathrm{B}}{2x^* L} J_1\left(\frac{x^* R}{R_\mathrm{B}}\right) \tag{19}$$

$$b_{1Z} = B_1 J_0\left(\frac{x^* R}{R_\mathrm{B}}\right) \tag{20}$$

$$J_\theta(R, Z_0) = \frac{B_1 c x^*}{4\pi R_\mathrm{B}}\left(1 - \left(\frac{R_\mathrm{B}}{2x^* L}\right)^2\right) J_1\left(\frac{x^* R}{R_\mathrm{B}}\right) \tag{21}$$

with $R \leq R_\mathrm{B}$. Here $R_\mathrm{B}$ is the radial distance from $R = 0$ to the point at which the field lines return to the base of the middle chromosphere. An example of this field is shown in Fig. 1. $J_0$ and $J_1$ are the Bessel functions of zero and first order, and $x^*(\sim 3.832)$ is the first zero of $J_1(x)$. $B_1$ is the maximum magnitude of the field. An equation for $B_1$ in terms of inputs to the model is given in Sect. 4.3.

The potential magnetic field is obtained by requiring that it be curl free and divergence free, and by assuming it has the $Z$ dependence given in Eqs. (15) and (16). It follows that the radial dependence of the $R$ and $Z$ components of the potential magnetic field is given by

$$b_{2R} = B_2\, J_1\left(\frac{R}{2L}\right) \tag{22}$$

$$b_{2Z} = B_2\, J_0\left(\frac{R}{2L}\right) \tag{23}$$

where $B_2$ is the maximum magnitude of the potential field. The value of $B_2$ is determined from the inputs to the model in the following way. Substitute Eqs. (8) and (21) for the resistivity and current density into the energy equation (12). Perform the integration with respect to $Z$, average the result over the area $\pi R_\mathrm{B}^2$ of the base of the magnetic element, and solve for $B_2$ to obtain

$$B_2 = \pm \frac{1}{{\Gamma_2}^{1/2}}\left(\frac{\Gamma_3}{{B_1}^2} - \Gamma_1\right)^{1/2} - B_1 \tag{24}$$

where

$$\Gamma_1 = (n_{\mathrm{H}0}\sigma)^2 \frac{k_\mathrm{B} T(0)}{m_\mathrm{p}} \tag{25}$$

$$\Gamma_2 = \left(\frac{e}{m_\mathrm{p} c}\right)^2 \tag{26}$$

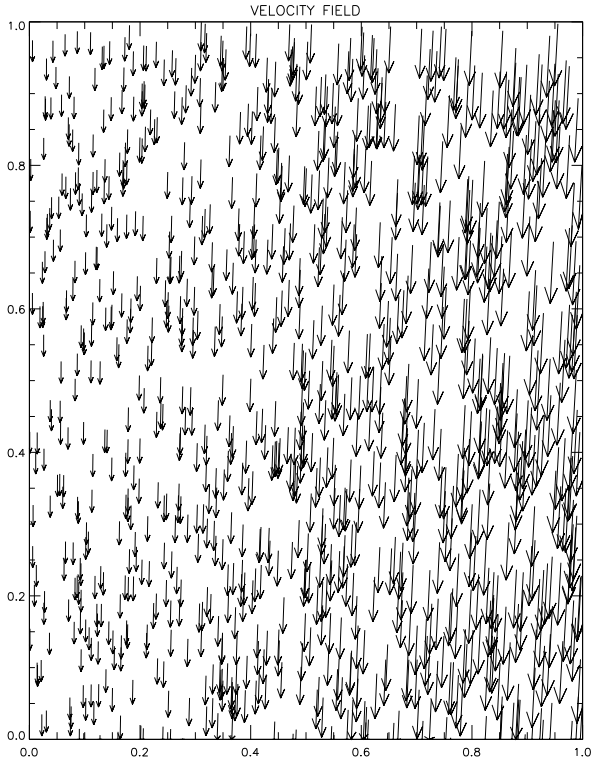


**Fig. 4.** Velocity vectors of the velocity field of solution b. The axis definitions and normalizations are the same as for Fig. 1. The length of the vectors is proportional to the flow speed. The velocity field of solution a has the same basic geometry.

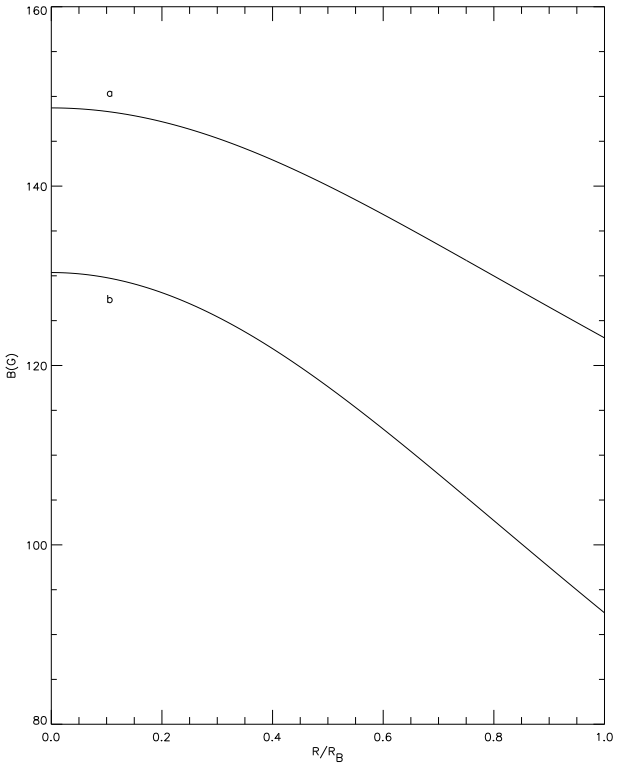


**Fig. 5.** Magnitude of the total magnetic field vs. $R/R_B$. The scale height of $B$ is 1800 km for both solutions. The average values of $B$ for solutions a and b are 134.1 and 108.8 G.

$$\Gamma_3 = \frac{< F > \sigma n_{\rm p0} n_{\rm H0}}{.162L} \left(\frac{k_{\rm B}T(0)}{{m_{\rm p}}^3}\right)^{1/2} \times \left(\frac{4\pi R_{\rm B} e}{x^* c} \frac{(2x^*L)^2}{((2x^*L)^2 - {R_{\rm B}}^2)}\right)^2 . \quad (27)$$

Here $n_{\rm H0} = n_{\rm H}(0, Z_0)$, $n_{\rm p0} = n_{\rm p}(0, Z_0)$, and $< F >$, which is an input to the model, is the average of the radiation flux $F(R)$ over the area $\pi {R_{\rm B}}^2$ of the base of the magnetic element. Solutions are found only for the choice of the positive root in Eq. (24). Combining Eq. (24) with Eq. (39) determines $B_2$ and $B_1$ in terms of the inputs to the model, discussed in Sect. 5.

## 4. Equations for numerical solution

### *4.1. Differential equations*

Let $r = R/L$. Then the differential equations to be solved are as follows.

$$\frac{{\rm d}v_R}{{\rm d}r} = \frac{1}{b_Z}\left\{\left(\frac{b_Z}{2} - \frac{b_R}{r}\right) v_Z + \frac{v_R}{2}\left(\left(\alpha^2 - 1\right) b_{1R} + b_R\right) - \frac{c^2\eta\left(\alpha^2 - 1\right)}{8\pi L}\left(\frac{b_{1Z}}{2} - \frac{b_{1R}}{r}\right) + \frac{b_R}{v_R}\left\{\frac{Lv_Z^2}{L_{\rm V}} + \frac{1}{\rho_0}\left[p_0 - \frac{LJ_\theta b_R}{c} - L\rho_0 g\right]\right\}\right\} \quad (28)$$

$$\frac{{\rm d}\rho_0}{{\rm d}r} = \rho_0\left[-\frac{1}{v_R}\frac{{\rm d}v_R}{{\rm d}r} - \frac{1}{r} + \frac{b_Z}{b_R} + \frac{c^2\eta(\alpha^2 - 1)}{8\pi L}\frac{b_{1R}}{v_R b_R}\right] \quad (29)$$

$$\frac{{\rm d}p_0}{{\rm d}r} = -\rho_0 v_R\left(\frac{{\rm d}v_R}{{\rm d}r} - \frac{Lv_Z}{L_{\rm V}}\right) + \frac{LJ_\theta b_Z}{c} \quad (30)$$

where $\alpha = 2Lx^*/R_{\rm B}$, $v_R(0) = 0$, and

$$v_Z = \frac{1}{b_R}\left(v_R b_Z + c\eta J_\theta\right) \quad (31)$$

with $J_\theta$ given by Eq. (21).

### *4.2. Constraints*

Requiring that all physical quantities be finite at $r = 0$ leads to the following constraints:

$$\left.\frac{{\rm d}v_R}{{\rm d}r}\right|_{r=0} = -\frac{c^2\eta(\alpha^2 - 1)B_1}{16\pi L(B_1 + B_2)} \quad (32)$$

$$\left.\frac{{\rm d}\rho_0}{{\rm d}r}\right|_{r=0} = 0 \quad (33)$$

$$\left.\frac{{\rm d}p_0}{{\rm d}r}\right|_{r=0} = 0 \quad (34)$$

$$v_Z(0) = 2\left.\frac{{\rm d}v_R}{{\rm d}r}\right|_{r=0} \quad (35)$$

$$v_Z(0) = \pm L_{\rm V}^{1/2}\left(g - \frac{p_0(0)}{L\rho_0(0)}\right)^{1/2} . \quad (36)$$

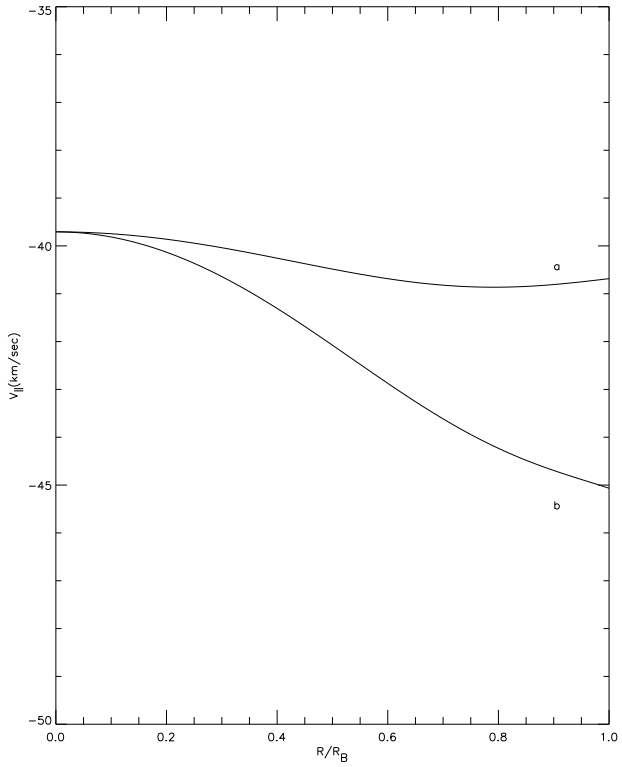


**Fig. 6.** Component of velocity parallel to $\boldsymbol{B}$ vs. $R/R_B$. The scale height of $V_\parallel$ is 7200 km for both solutions. The average values of $V_\parallel$ for solutions a and b are -40.6 and -43.2 km-sec$^{-1}$.

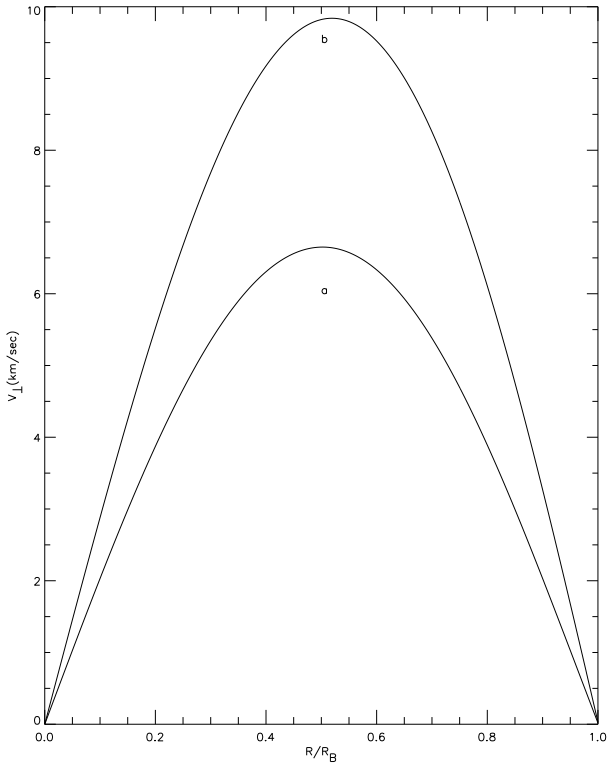


**Fig. 7.** Component of velocity perpendicular to $\boldsymbol{B}$ vs. $R/R_B$. The scale height of $V_\perp$ is 7200 km for both solutions. The average values of $V_\perp$ for solutions a and b are 4.2 and 6.4 km-sec$^{-1}$.

In order that $v_Z(0)$ be real it is necessary that

$$L \geq \frac{p_0(0)}{\rho_0(0)g} \tag{37}$$

Solutions are found only for $v_Z(0) < 0$.

Requiring that the pressure increase with $r$ near $r$ = 0 implies that the condition

$$R_{\rm B} < 2Lx^* \tag{38}$$

must hold. This is also found to be a sufficient condition. This constraint is one of two constraints on $R_{\rm B}$. The second one is given by Eq. (41).

### *4.3. Equation for $B_1$*

Combining Eqs. (24), (32) and (35), and solving for $B_1$ neglecting terms of relative order $(\omega_{\rm p}\tau_{\rm pH})^{-2}$ gives

$$B_1 = \pm\left(\frac{\Gamma_3 - \Gamma_2\Gamma_4^2}{\Gamma_1}\right)^{1/2} \tag{39}$$

where

$$\Gamma_4 = -\frac{\sigma n_{\rm p0}(\rho_0(0)p_0(0))^{1/2}8\pi L v_Z(0)}{(\alpha^2-1)}. \tag{40}$$

This is the only place in the model where it is assumed that $(\omega_{\rm p}\tau_{\rm pH})^2 \gg 1$. The justification for this assumption is that the protons are found to be magnetized for the solutions discussed in Sect. 5.

Solutions are found only for $B_1 > 0$. In order that $B_1$ be real it is necessary that

$$R_{\rm B} \leq \frac{x^*}{\left|\frac{{\rm d}v_R}{{\rm d}r}\right|_{r=0}}\left(\frac{< F > L}{.162\sigma n_{\rm p0}n_{\rm H0}\left(m_{\rm p}k_{\rm B}T(0)\right)^{1/2}}\right)^{1/2} \tag{41}$$

which is the second constraint on $R_{\rm B}$. Here ${\rm d}v_R/{\rm d}r$ at $r$ = 0 is given by Eq. (32).

## 5. Particular solutions

The procedure for generating a solution is as follows. Specify $T(0)$, $n_{\rm H0}$, $n_{\rm p0}$, $\sigma$, and $< F >$. Compute $p_0(0)$ using the ideal gas law (11). Choose $L$ subject to the constraint (37). Choose $L_{\rm V} \gg L$. Compute $v_Z(0)$ using Eq. (36). Compute ${\rm d}v_R/{\rm d}r$ at $r$ = 0 using Eq. (35). Choose $R_{\rm B}$ subject to the constraints (38) and (41). Compute $B_1$ and $B_2$ using Eqs. (24) and (39). Compute $\eta$ using Eq. (8). Solve the differential Eqs. (28) - (30). All other quantities are determined algebraically once $V_R, p,$ and $\rho$ are known.

Two solutions labeled a and b are presented in Figs. 1 - 14. For these solutions $< F >$, $T(0)$, $L$, $L_{\rm V}$, and $n_{\rm p0}$ are fixed at $2 \times 10^7$ ergs-cm$^{-2}$-sec$^{-1}$, 6000 K, 900 km, 7200 km, and $10^7$ cm$^{-3}$. The remaining inputs for solutions a and b

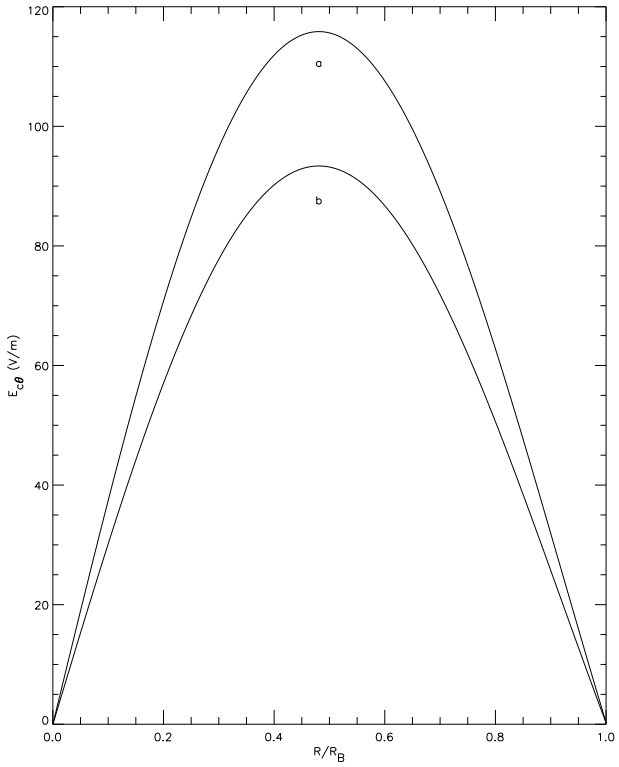


**Fig. 8.** Convection electric field vs. $R/R_B$. The scale height of $E_{c\theta}$ is the same as for $B$ in Fig. 5. The average values of $E_{c\theta}$ for solutions a and b are 57.6 and 71.5 V-m$^{-1}$.

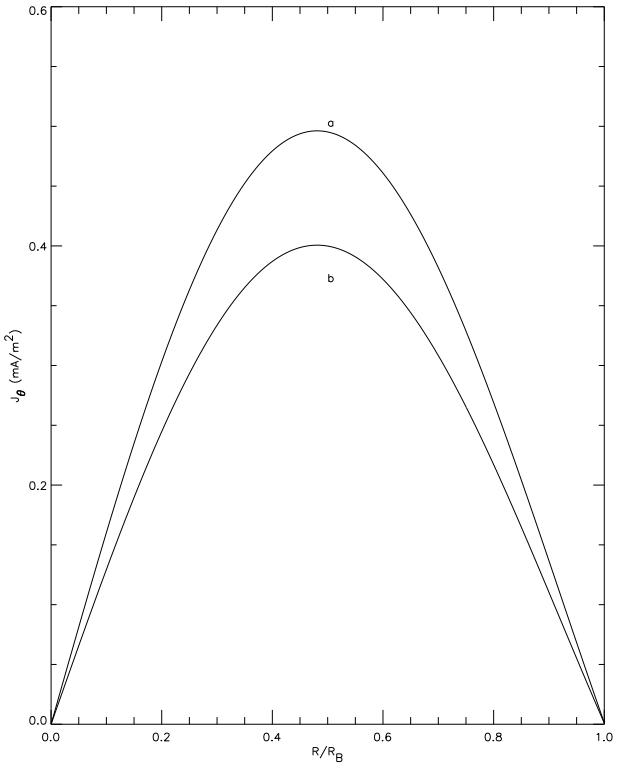


**Fig. 9.** Current density vs. $R/R_B$. The scale height of $J_\theta$ is the same as for $B$ in Fig. 5. The average values of $J_\theta$ for solutions a and b are .31 and .25 mA-m$^{-2}$.

are $(R_{\rm B}({\rm km}), n_{\rm H0}({\rm cm}^{-3}))$ = $(1873, 2 \times 10^{13})$ and $(2651, 10^{13})$. There are three criteria used to generate a solution. First, the maximum magnetic field strength $B_1 + B_2$ is required to be under 200 G. The maximum field strength is attained at $R$ = 0 at the base of the middle chromosphere, defined as being at $Z = Z_0$. Second, the average value of the heating rate per unit mass is required to be close to the value $4.5 \times 10^9$ ergs-g$^{-1}$-sec$^{-1}$ obtained by Anderson & Athay (1989a). Third, the maximum temperature is required to be less than 9000 K.

Figs. 1-4 show the geometry of the loop shaped non - potential magnetic element, potential magnetic field, total magnetic field, and hydrogen flow velocity for solution b. The basic geometry of these fields is the same for solution a. For solution a the maximum potential and non - potential field strengths are 143.1 G and 5.7 G. For solution b they are 123.3 G and 7.0 G. Hence the non - potential field is 18 - 25 times weaker than the potential field so that Figs. 2 and 3 are nearly identical. The magnetic element is embedded in a much stronger, larger scale potential field. The hydrogen flows downward and towards the central region of the magnetic element, near $R$ = 0, where the field is strongest and mainly vertical. Since, as discussed below, $\boldsymbol{V}$ is nearly parallel to $\boldsymbol{B}$, the streamlines in Fig. 4 are nearly the same as the magnetic field lines in Fig. 3.

Figs. 5-14 show plots of quantities at the base of the middle chromosphere. The scale heights for all quantities, and their averages over the base area $\pi R_{\rm B}^2$ of the magnetic element, are given in the figure captions.

Fig. 5 shows the magnitude of $\boldsymbol{B}$. The field is strongest near $R$ = 0, and decreases in magnitude as the field lines flare out from the central region of mainly vertical field. In the photospheric network, flux tubes with field strengths of $\sim 1 - 2$ kilogauss and diameters $\sim 1''$ or less are observed (Lin 1995; Solanki 1993). In the photospheric internetwork, magnetic flux tubes with an average field strength of 500 G and diameters of 100 km or less are observed (Lin 1995, Keller et al. 1994). The field lines of some of these flux tubes extend into the middle chromosphere and return to the photosphere. These flux tubes are identified here as the photospheric roots of the magnetic elements in the model. The diameter of the flux tubes expands with height, and field lines flare out in the horizontal direction spanning a region in the middle chromosphere much greater than the diameter of the flux tubes in the photosphere before returning to the photosphere as a weaker, relatively diffuse field of opposite polarity.

Figs. 6 and 7 show the components of $\boldsymbol{V}$ parallel and perpendicular to $\boldsymbol{B}$. The flow is mainly parallel to $\boldsymbol{B}$. The average flow speed is $\sim$ 40 km-sec$^{-1}$. There does not appear to be any observational evidence for downflows with speeds as high as 40 km-sec$^{-1}$ in the quiet middle chromosphere, although downflows with speeds up to 10 km-sec$^{-1}$ are observed in H$\alpha$ in the quiet network (Heinzel & Schmieder 1994). Therefore the flow

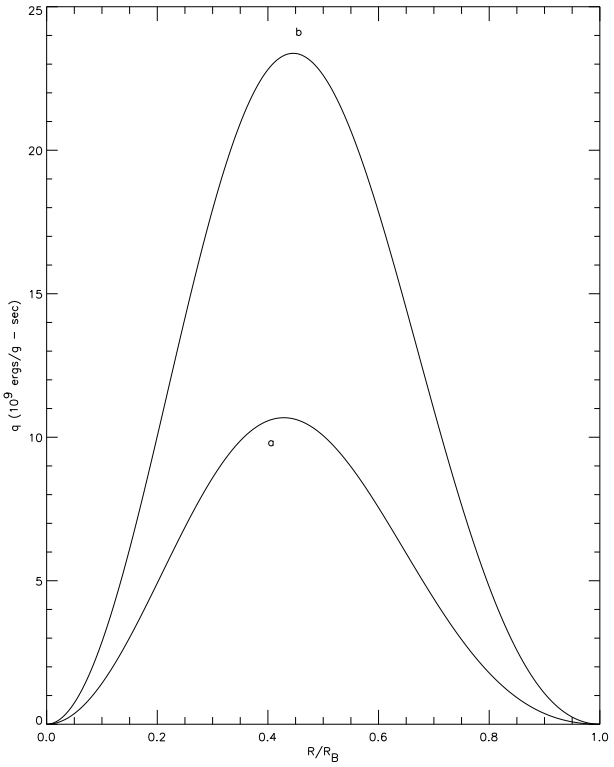


**Fig. 10.** Heating rate per unit mass vs. $R/R_B$. $q$ is independent of height. The average values of $q$ for solutions a and b are $(4.5, 10.2)\times 10^9$ ergs-g$^{-1}$-sec$^{-1}$.

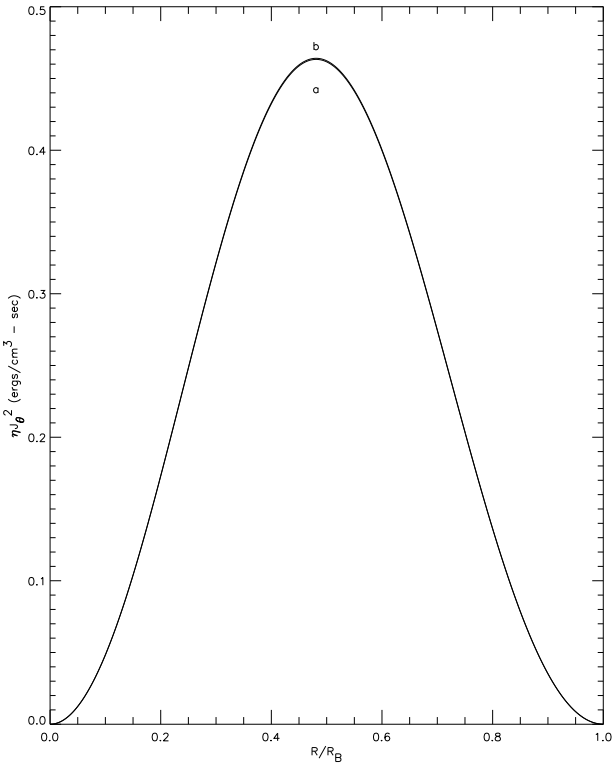


**Fig. 11.** Heating rate per unit volume vs. $R/R_B$. The scale height of $\eta {J_\theta}^2$ is the same as for the pressure in Fig. 13. The average value of $\eta {J_\theta}^2$ for solutions a and b is .222 ergs-cm$^{-3}$-sec$^{-1}$.

speeds predicted by the model are about a factor of four too high with respect to the quiet middle chromospheric network. However, there is observational evidence for high speed downflows in magnetic loops in active regions of the middle chromosphere as seen in H$\alpha$ (Bruzek 1967, 1969; Chou & Zirin 1988; Roberts 1970; Zwann et al. 1985). The speed of these downflows ranges from 25 to 50 km-sec$^{-1}$, and the horizontal spatial scale of the magnetic loops is 1 - 5 arcseconds. In addition, systems of these loops may cover an entire supergranulation cell with plasma streaming downwards at the boundary of the cell where the chromospheric network is located (Bruzek 1969). There is a strong spatial correlation between these loops and bright points (i.e. heating) as discussed by Bruzek (1967). Therefore the range of downflow speeds predicted by the model to occur in heated magnetic loops is consistent with downflow speeds observed in magnetic loops of the same size in active regions, where the most intense heating takes place. This suggests that the proposed heating mechanism may at least be useful in understanding how the middle chromosphere is heated in active regions.

Magnetic loops are observed to rise through the middle chromosphere at speeds of 7 - 20 km-sec$^{-1}$ (Zwann et al. 1985; Chou & Zirin 1988; Bruzek 1967, 1969). The relative motion of the loops and the surrounding plasma causes some of the plasma to be driven across magnetic field lines, thereby causing some heating by the proposed heating mechanism.

In fibrils and spicules flow speeds up to 40 km-sec$^{-1}$ are observed in the upper chromosphere, with the fibril flow being mainly horizontal, and the spicule flow being mainly vertical (Suematsu et al. 1995; Athay 1981). There appears to be a strong causal connection between bright points, spicules, and the magnetic field in the lower chromospheric network (Suematsu et al. 1995). Return flow from spicules is expected to have a component orthogonal to the magnetic field, causing heating by the proposed heating mechanism. The flow observed in fibrils and spicules may be mostly aligned with the horizontal and vertical components of magnetic loops, with a relatively small component of flow orthogonal to the field.

Flows in the photospheric network outside of spicules and near magnetic flux tubes tend to be downward with speeds up to $\sim$ 3 km-sec$^{-1}$ (Solanki 1993). There may be a connection between these downflows and those predicted by the model to occur higher in the atmosphere in magnetic structures that are rooted in flux tubes in the underlying photosphere.

The relatively small component of flow orthogonal to $\boldsymbol{B}$ is sufficient to generate a convection electric field, shown in Fig. 8, which drives the current density, shown in Fig. 9, that through resistive dissipation generates the required average heating rate $< F >= 2\times 10^7$ ergs-cm$^{-2}$-sec$^{-1}$. The electric field and current density are related by the scale factor $\eta$. For solutions a and b $\eta = 2.1 \times 10^{-5}$ sec and $3.2 \times 10^{-5}$ sec.

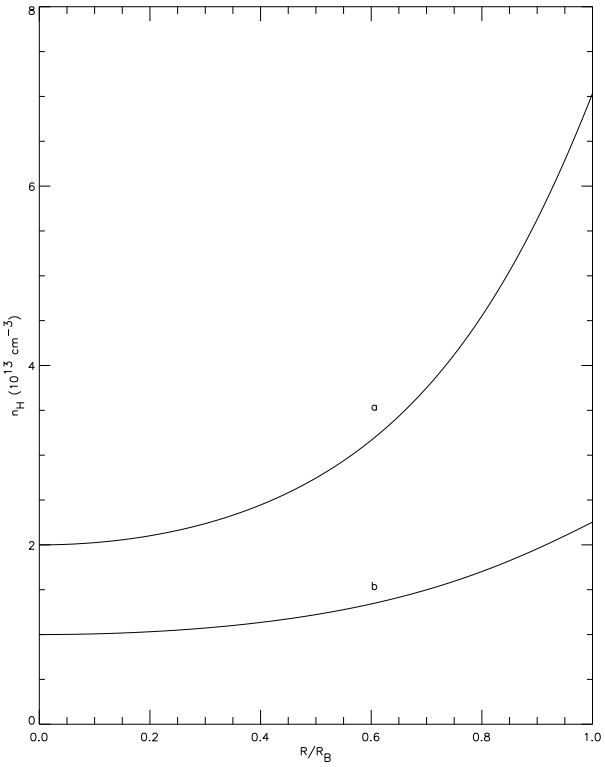


**Fig. 12.** Hydrogen density vs. $R/R_B$. The scale height of $n_{\rm H}$ is the same as for the pressure in Fig. 13. The average values of $n_{\rm H}$ for solutions a and b are $(4.1, 1.6) \times 10^{13}$ cm$^{-3}$.

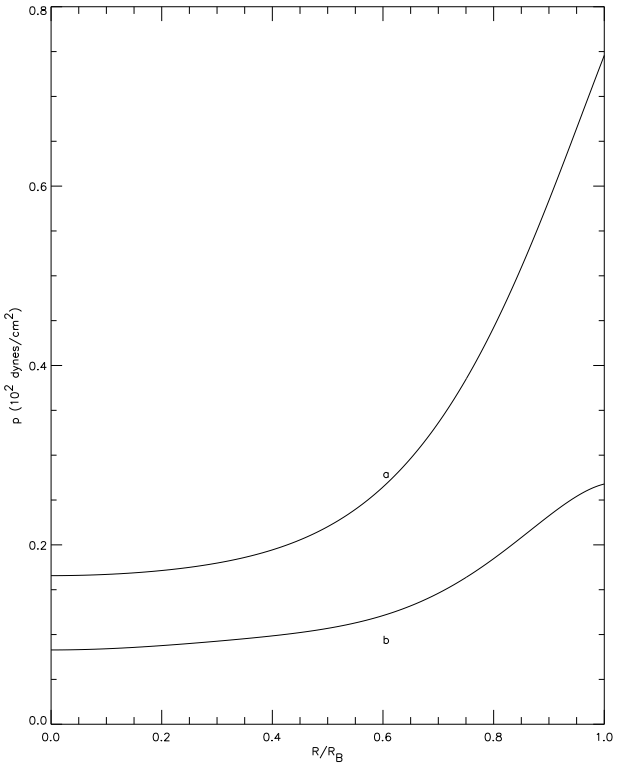


**Fig. 13.** Pressure vs. $R/R_B$. The scale height of $p$ for solutions a and b is 900 km. The average values of $p$ for solutions a and b are 38.5 and 16.2 dynes-cm$^{-2}$.

The heating rates per unit mass and volume are shown in Figs. 10 - 11. They reach their maximum values near the middle of the magnetic element where its magnetic field is mainly horizontal. Hence most of the emitted radiation is expected to come from a region of the magnetic structure displaced horizontally from the region near $R$ = 0 where the magnetic field is strongest and mainly vertical. Since the potential field is about twenty times stronger than the non - potential loop shaped field of the magnetic element, magnetograms of bright magnetic loops in the middle chromosphere may suggest that the field is potential, and hence current free, possibly leading to the erroneous conclusion that resistive heating is not important.

The hydrogen density and pressure are shown in Figs. 12 and 13. The smaller magnetic structure of solution a has a higher pressure and density than those of solution b. The central regions of these structures, similar to the inside of a flux tube, have a lower pressure and density than the outside region.

The temperature is shown in Fig. 14. The temperature is no greater than 8700 K, and almost always remains within the middle chromospheric temperature range of $6000 - 8000$ K predicted by semi - empirical models (Anderson & Athay 1989a,b; Avrett 1984; Vernazza et al. 1981). The temperature varies little in the region where the heating rates increase from zero at $R$ = 0 to their maximum values near $R = R_{\rm B}/2$, but increases rapidly in the region $R > R_{\rm B}/2$. As the heating rates increase over the interval from $R$ = 0 to $R \sim R_{\rm B}/2$ the increase in density causes the temperature to remain approximately constant despite the increase in the thermal energy density $3p/2$. In other words, over this interval the rate of thermal energy generation is increasing but the energy is being distributed over an increasing number of particles such that the energy per particle remains approximately constant. In the region $R > R_{\rm B}/2$ the rapid increase in the horizontal pressure gradient compresses the plasma causing the temperature to increase. The result that the temperature is almost constant from $R$ = 0 to $R \sim R_{\rm B}/2$ suggests that a large horizontal variation in net radiative loss may not always be associated with a large horizontal variation in temperature.

Rewriting Eq. (36) as

$$\frac{\rho_0(0) v_Z^2(0)}{L_{\rm V}} + \frac{n_{\rm H0} k_{\rm B} T(0)}{L} = \rho_0(0) g. \tag{42}$$

shows that near $R$ = 0 the vertical component of the inertial force generated by the height variation of the velocity supports the plasma against gravity. This allows for a lower temperature for a given number density.

The average values of $\beta$ for solutions a and b are 6% and 4%. The corresponding maximum values of $\beta$ are 13% and 8%.

## 6. Conclusions

It is possible that a significant source of heating for magnetic loops with diameters up to at least $\sim 4''$ in the middle chromo-

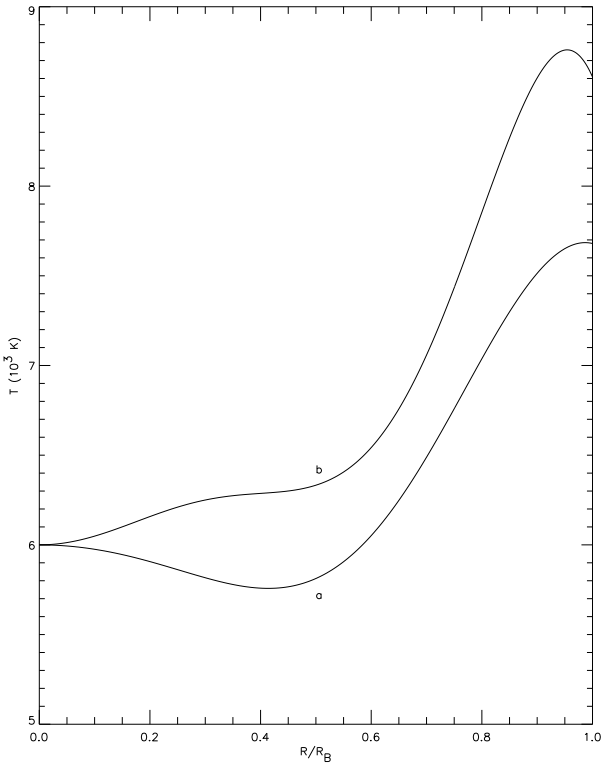


**Fig. 14.** Temperature vs. $R/R_B$. $T$ is independent of height. The average values of $T$ for solutions a and b are 6629 and 7328 K.

sphere is resistive dissipation of currents driven by a convection electric field generated by the flow of weakly ionized hydrogen across the magnetic field. Any process which drives flow across the magnetic field, such as any of the processes mentioned at the end of Sect. 1, leads to heating by this mechanism.

Inertial forces are important in maintaining force balance in the middle chromosphere. In particular, it is necessary to allow for the variation of flow velocity with height when modeling heating of the middle chromosphere by the resistive heating mechanism proposed here in order to obtain realistic values of the temperature.

Including the variation of flow velocity with height in the formulation used here leads to reasonable temperature profiles for magnetic structures with horizontal spatial extents of $\sim 1900 - 2700$ km. The generation of these profiles provides support for the claim that the proposed heating mechanism is important for heating magnetic loops confined to the middle chromospheric network. Acceptable solutions for much larger structures do not appear to be allowed by the model. This restriction may be due to the simple manner in which the variation of flow velocity with height is taken into account. It remains to be seen whether a more realistic model can recover the much larger structures having $R_{\rm B} \sim 1 - 3 \times 10^4$ km obtained and discussed by Goodman (1997). The recovery of these larger structures is important in order to support the proposition in Goodman (1997) that they form the building blocks of the chromospheric magnetic canopy, and that the proposed heating mechanism makes a major contribution to middle chromospheric heating in the internetwork.

The temperature profiles for the magnetic structures discussed in Sect. 5 indicate that there is little horizontal variation in temperature between the central, flux tube shaped region where the magnetic field is strongest and the heating rates are smallest, and the region where the heating rates are largest. This suggests that observations with spatial resolution high enough to resolve the structure of heated magnetic loops in the middle chromosphere may not reveal a strong correlation between large horizontal variations in net radiative loss and horizontal variations in temperature. The highest temperatures may occur in the outer region of the loops where $R \sim R_{\rm B}$, the heating rates are small, the magnetic field is relatively weak and diffuse, and compression due to the horizontal gradient of the gas pressure is largest.

The model generated temperature profiles lie in the range which characterizes the middle chromosphere. However, these profiles must be viewed with caution since the model uses the simplest form of an energy equation which balances resistive heating with net radiative loss. The most important step towards making the energy equation more realistic is to replace the function $F(R)$ which represents the net radiative loss, and which has an average value that is specified, by an expression which is a function of temperature, and electron, proton, and hydrogen densities. Since a large number of spectral lines dominate the net radiative loss in the middle chromosphere, and since most of these lines are formed far out of thermodynamic equilibrium, either an approximate representation must be used for these losses, or a large number of radiative transfer equations must be solved simultaneously with the other equations of the MHD model. The latter approach is very difficult in the context of a two dimensional MHD model. The use of an alternative approximate representation of the net radiative losses that allows for their self consistent calculation is a high priority for future modeling.

*Acknowledgements.* The author thanks Stuart Jordan in the Laboratory for Astronomy and Solar physics at NASA Goddard for important discussions of the material presented in this paper. The author also thanks Steven Curtis and William Mish in the Laboratory for Extraterrestrial Physics at NASA Goddard for their support of this work.

## References

Anderson, L.S. & Athay, R.G. 1989a, ApJ, 336, 1089
Anderson, L.S. & Athay, R.G. 1989b, ApJ, 346, 1010
Athay, R.G. 1981, in The Sun as a Star, ed. S.D. Jordan (NASA SP-450), 85
Avrett, E.H. 1984, in Chromospheric Diagnostics and Modeling, ed. B.W. Lites (Sunspot, NM: National Solar Observatory)
Bocchialini, K., Vial, J - C & Koutchmy, S. 1994, ApJ, 423, L67
Book, D.L. 1994, NRL Plasma Formulary (Naval Research Laboratory), 39
Bruzek, A. 1967, Sol. Phys., 2, 451
Bruzek, A. 1969, Sol. Phys., 8, 29
Carlsson, M. & Stein, R.F. 1992, ApJ, 397, L59

Carlsson, M. & Stein, R.F. 1994, in Chromospheric Dynamics, ed. M. Carlsson (Inst. of Theoretical Astrophysics, University of Oslo, Norway), 47
Carlsson, M. & Stein, R.F. 1995, ApJ, 440, L29
Chapman, S. & Cowling, T.J. 1970, The Mathematical Theory of Non-Uniform Gases (Cambridge), 366
Chou, D.Y. & Zirin, H. 1988, ApJ, 333, 420
Deubner, F. - L. & Fleck, B. 1990, A&A, 228, 506
Goodman, M.L. 1995, ApJ, 443, 450
Goodman, M.L. 1996, ApJ, 463, 784
Goodman, M.L. 1997, A&A, in press.
Heinzel, P. & Schmieder, B. 1994, A&A, 282, 939
Kalkofen, W. 1996, ApJ, 468, L69
Keller, C.U., Deubner, F. - L., Egger, U., Fleck, B. & Povel, H.P. 1994, A&A, 286, 626
Kneer, F. & von Uexküll, M. 1993, A&A, 274, 584
Kulaczewski, J. 1992, A&A, 261, 602
Lin, H. 1995, ApJ, 446, 421
Lites, B.W. 1994, in Chromospheric Dynamics, ed. M. Carlsson (Inst. of Theoretical Astrophysics, University of Oslo, Norway), 1
Lites, B.W., Rutten, R.J. & Kalkofen, W. 1993, ApJ, 414, 345
Rammacher, W. & Ulmschneider, P. 1992, A&A, 253, 586
Roberts, P.H. 1970, Ph.D. thesis, California Institute of Technology
Sivaraman, K.R. & Livingston, W.C. 1982, Sol. Phys., 80, 227
Solanki, S.K. 1993, Space Science Rev., 63, 1
Solanki, S.K., Bruls, J.H.M.J., Steiner, O., Ayres, T., Livingston, W. & Uitenbroek, H. 1994, in Solar Surface Magnetism, R.J. Rutten & C.J. Schrijver (eds.), NATO ASI Series C433, Kluwer, Dordrecht, 91
Suematsu, Y., Wang, H. & Zirin, H. 1995, ApJ, 450, 411
Ulmschneider, P., E.R. Priest & R. Rosner (eds.) 1991, Mechanisms of Chromospheric and Coronal Heating (Berlin: Springer)
Vernazza, J.E., Avrett, E.H. & Loeser, R. 1981, ApJS, 45, 635
von Uexküll, M. & Kneer, F. 1995, A&A, 294, 252
Zwann, C., Brants, J.J. & Cram, L.E. 1985, Sol. Phys., 95, 3

This article was processed by the author using Springer-Verlag LaTeX A&A style file *L-AA* version 3.